Cement and Concrete Research 39 (2009) 45–53

Contents lists available at ScienceDirect

Cement and Concrete Research

journal homepage: http://ees.elsevier.com/CEMCON/default.asp

The mineralogy of the $CaO–Al_2O_3–SiO_2–H_2O$ (CASH) hydroceramic system from 200 to 350 °C

Nicola Meller, Konstantinos Kyritsis, Christopher Hall *

Centre for Science at Extreme Conditions and School of Engineering & Electronics, The University of Edinburgh, The King's Buildings, Edinburgh EH9 3JL, UK

ARTICLE INFO

Article history:
Received 23 April 2008
Accepted 7 October 2008

Keywords:
Hydration products
X-ray diffraction
Oil well cement
Geothermal well cement

ABSTRACT

We describe a quantitative mineralogical study of the hydrothermal reactions of an oil well cement with added silica and alumina, hydrated at temperatures from 200 to 350 °C. We compare the products with pure end member systems and find phase stability can be altered radically, even by small amounts of additive. The upper temperature limits of α-C_2SH (<250 °C), and 1.1 nm tobermorite $C_5S_6H_5$ (<300 °C) are increased. C_8S_5, reported in a cement-based system for the first time, is stable to 300 °C and is believed to prevent foshagite C_4S_3H formation below 350 °C. Hydrogarnet $C_3AS_{3-y}H_{2y}$ is the only aluminum bearing phase at <300 °C but it coexists with $C_4A_3H_3$ and bicchulite $C_8A_4Si_4H_4$ at higher temperatures. The presence of alumina increases the stability of 1.1 nm tobermorite greatly and also to a lesser degree of gyrolite.

1. Introduction

Various potential sources of geothermal energy exist in many regions, for example in the UK in the form of radiothermal granites [1–5]. In geothermal systems, cool fluids are pumped down an injection well, heated at depth by the surrounding rock formation and returned to surface via a production well. Such methods, formerly known as hot dry rock (HDR) technology and now as enhanced geothermal systems (EGS), require the annulus between the well casing and rock formation to be sealed with cementitious materials to prevent the escape of the working fluid in much the same way as an oil or gas well is sealed [6]. This paper reports a detailed examination of the mineralogy of sealants based on an oil well cement with additions of silica and alumina for use in geothermal wells over the temperature range 200 to 350 °C. The engineering properties of these sealants are described elsewhere [7].

In oilfield engineering, it is standard practice to use special cement formulations when the well temperature exceeds 110 °C. Above this temperature the predominant phase formed in the simple hydration of an oilwell cement is α-dicalcium silicate hydrate α-C_2SH[1] [$Ca_2SiO_3(OH)_2$], which forms bulk materials that are too weak and permeable to seal the well [6,8]. On initial hydration cement first forms a C–S–H gel which on heating converts to crystalline α-C_2SH. This crystallization causes a reduction in solid volume and is accompanied by an increase in permeability and the reduction in compressive strength known as *strength retrogression*.

Therefore silica is commonly added to cement (typically approx 35% by wt of cement BWOC) to reduce the C/(C+S) mol ratio to about 0.5. This prevents the formation of α-C_2SH and instead numerous other crystalline calcium silicate hydrates are produced. Fig. 1 redraws the well known summary diagram of Taylor [9] based on information available in 1964 which shows the hydrates commonly found under various conditions. We emphasize, as did Taylor, that these are not necessarily the equilibrium phases. Such cement + silica formulations often yield bulk materials with greater strength and lower permeability than cement alone. While such formulations are normally acceptable for oil wells they are not always durable in the hostile chemical environments encountered in geothermal wells, and formation damage or sealant deterioration or both can occur.

With high temperature well cementing in mind, Barlet-Gouédard et al. [10,11] and Meller et al. [12–14] have recently designed hydroceramics based on the $CaO–Al_2O_3–SiO_2–H_2O$ (CASH) system at 200 and 300 °C. A hydroceramic is defined here as any ceramic composition containing chemically combined water as H_2O or OH or both. The studies carried out by Barlet-Gouédard et al. used the principle, first described by Roy et al. [15–17], that the sealant should have the same overall chemical composition as the surrounding rock formation: hence if the rock formation is stable in that environment the sealant should be too. For this reason a limited number of compositions was assessed. Our research extends the CASH system to cover a wider range of compositions and temperatures. A detailed knowledge of the mineralogy of a complete system delivers more options should some compositions be unsuitable in certain chemical environments. We describe here the detailed mineralogy of a suite

* Corresponding author.
E-mail address: christopher.hall@ed.ac.uk (C. Hall).

[1] Note that cement nomenclature will be used generally throughout: C = CaO, S = SiO_2, A = Al_2O_3, F = Fe_2O_3, H = H_2O, $\bar{S}$ = SO_3, $\bar{C}$ = CO_2. The complete chemical formula of each individual mineral is given in Table 4.

0008-8846/$ – see front matter © 2008 Elsevier Ltd. All rights reserved.
doi:10.1016/j.cemconres.2008.10.002

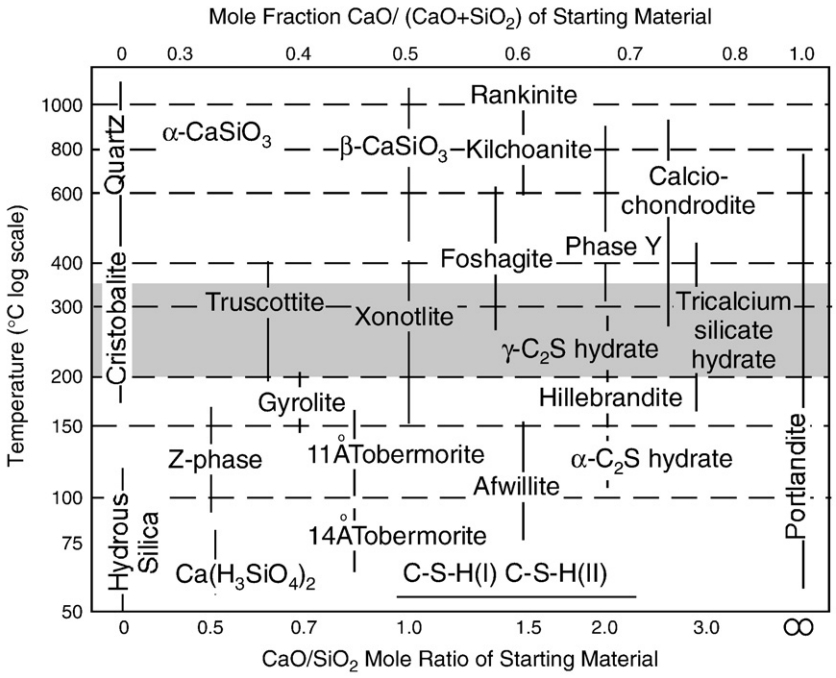

Fig. 1. $CaO–SiO_2–H_2O$ phases from 50 to 1000 °C. After Taylor [9], with modifications. The vertical lines indicate the C/S mole ratios of the phases. As emphasized by Taylor, this is not an equilibrium diagram, but "merely represents the conditions under which each phase is most usually obtained". The grey shaded area illustrates the temperature range covered by this study (200 to 350 °C).

of hydroceramic compositions over the temperature range 200 to 350 °C. We have used X-ray diffraction to determine the mineralogical composition and Rietveld refinement to quantify the phases present at different temperatures. This information is drawn together into a model of the CASH system at temperatures typical of geothermal wells. Ground-breaking work on compositions within the hydrothermal CASH system and their properties was carried out by Roy et al. [17], using both cements and lime as the source of CaO. The effects of alkalis and magnesium oxide additions were also investigated [16].

2. Experimental

Dyckerhoff oilwell cement (API Class G) was used as the basis of the hydroceramics investigated. This commercial cement is widely used in well construction and has a consistent composition. The oxide analysis of the cement and the calculated mineralogical composition are summarized in Table 1. The mineralogy from a modified Bogue calculation [18] developed for oil well cements is in rather good agreement with that estimated by Rietveld whole-pattern fitting (mean of ten independent measurements) using Bruker TOPAS software. Silica was added in the form of silica flour HPF6, supplied by Sibelco, and composed of 98% silica as quartz SiO_2 with trace impurities and a mean grain size of 53 µm. Reagent grade α-alumina (corundum Al_2O_3) with a grain size of 50 to 150 µm, supplied by Sigma Aldrich [product code 34271-8], was used as the primary source of Al_2O_3. Additional samples were synthesised using finer alumina in the form of polishing powder supplied by Buehler [product code 40-6305-008, grain size 0.3 µm].

A total of 10 g of the starting compounds in the appropriate proportions was mixed with 4 g of water (water to total solids weight ratio w/s=0.4). Table 2 gives all the different compositions investigated using coarse alumina. Table 3 lists the compositions using finer alumina. The results and discussion in this paper concern samples prepared with coarse alumina (Table 2) unless explicitly stated otherwise. Each sample paste was mixed by hand and loaded into a steel cup approx 3 cm dia by 1 cm high. Six of these cups were then stacked in a 125 mL capacity stainless steel pressure vessel (type 4750 Parr Instruments), rated at 200 bar at the maximum working temperature of 350 °C. Small notches in the rims of the steel cups prevent steam building up between samples and ensure a uniform water-saturated atmosphere throughout. Once sealed, the Parr cell was placed in an oven at the selected curing temperature in the range of 200 °C to 350 °C and left to hydrate for 5 d. After curing the Parr cell was removed from the oven and chilled rapidly in cold water to prevent further reaction. Samples were then left to dry in a vacuum to reduce carbonation before they were removed from the steel cups and milled to fine powders for XRD analysis. We recognise that systems do

Table 1
Chemical and mineralogical composition of Dyckerhoff Class G cement determined by X-ray fluorescence, LECO sulphur analysis and X-ray diffraction

Oxides	Weight %	
Na_2O	0.17	
MgO	0.76	
Al_2O_3	3.62	
SiO_2	22.55	
K_2O	0.66	
CaO	65.61	
TiO_2	0.17	
Mn_3O_4	0.14	
Fe_2O_3	4.53	
SO_3	1.82	
Loss on ignition at 1000 °C	1.18	
Free lime	0.40	
Insoluble residue	Not determined	
%Phases	By Modified Bogue method	By Rietveld refinement
Alite C_3S	62	60
Belite C_2S	21	22
Aluminoferrite $C_4(A,F)$	13 (A/F=0.72)	16
Gypsum $C\bar{S}H_2$	3	3

Wt.% phase compositions are calculated from oxide analysis according to the modified Bogue method for oilwell cements [18] and estimated by semi-quantitative Rietveld refinement.

Table 2
Weight percent of phases present in each sample as estimated by Rietveld refinement

Initial composition % BWOC		Wt.% of phases in hydroceramics			
Silica flour	Coarse corundum	200 °C	250 °C	300 °C	350 °C
0.0	0.0	*p*=8; *j*=74; *a*=18	*p*=5; *j*=76; *r*=19	*p*=14; *j*=36; *r*=34; *h*=16 (*y*=1.6)	*p*=18; *j*=20; *r*=47; *h*=15 (*y*=1.3)
5.3	0.0	*p*=8; *j*=32; *a*=60	*j*=32; *r*=68	*j*=16; *r*=68; *h*=15 (*y*=1.5)	*p*=1; *j*=8; *r*=77; *h*=14 (*y*=1.3)
11.1	0.0	*j*=9; *a*=6; *m*=49; *k*=27; *t*=9	*j*=2; *r*=6; *m*=84; *x*=8	*j*=2; *r*=11; *m*=74; *x*=12	*j*=10; *r*=68; f=8; *h*=14 (*y*=1.1)
17.6	0.0	*j*=4; *a*=7; *m*=66; *t*=11; *x*=13	*j*=2; *m*=85; *x*=13	*j*=4; *r*=15; *m*=51; *x*=30	*j*=11; *r*=27; *x*=62
25.0	0.0	*j*=1; l=4; *m*=37; *k*=10; *t*=16; *x*=31	*m*=82; *x*=18	*m*=73; *x*=27	*x*=100
33.3	0.0	*t*=15; *x*=85	*x*=100	*m*=60; *x*=40	*x*=100
42.9	0.0	*t*=8; *x*=92	*x*=100	*x*=98; *v*=2	*x*=60; *v*=40
53.9	0.0	*t*=18; *x*=92	*x*=59; *g*=13; *v*=29	*x*=71; *v*=29	*x*=26; *v*=74
66.7	0.0	*x*=36; *g*=59; *q*=6	*x*=18; *g*=56; *v*=26	*x*=35; *v*=65	*x*=10; *v*=90
81.8	0.0	*x*=22; *g*=65; *q*=13	*x*=5; *g*=64; *v*=26; *q*=5	*v*=98; *q*=2	*v*=91; *q*=9
100.0	0.0	*g*=70; *q*=30	*g*=64; *v*=21; *q*=21	*v*=88; *q*=12	*v*=84; *q*=16
0.0	5.3	*p*=7; *j*=44; *a*=9; *h*=40 (*y*=1.9)	*p*=3; *j*=42; *r*=7; *h*=47 (*y*=1.8)	*p*=10; *j*=30; *h*=61 (*y*=1.8)	*p*=15; *j*=16; *h*=69 (*y*=1.7)
0.0	11.1	*p*=6; *j*=30; *h*=64 (*y*=2.0)	*p*=5; *j*=8; *r*=7; *h*=87 (*y*=2.1)	*p*=7; *j*=17; *h*=76 (*y*=1.9)	*p*=12; *j*=6; *h*=82 (*y*=1.8)
0.0	17.6	*p*=5; *j*=13; *h*=82 (*y*=2.0)	*p*=5; *j*=8; *h*=87 (*y*=2.1)	*p*=5; *j*=7; *h*=88 (*y*=2.0)	*p*=5; *j*=4; *h*=81 (*y*=2.0); *d*=11
0.0	25.0	*j*=3; *h*=97 (*h*=2.1)	*j*=7; *h*=92 (*y*=2.1)	*j*=6; *h*=83 (*y*=2.1); *d*=11	*p*=1; *j*=3; *h*=72 (*y*=2.0); *b*=4; *d*=20
0.0	33.3	*j*=3; *h*=88 (*y*=2.2); *c*=9	*j*=7; *h*=82 (*y*=2.1); *c*=11	*j*=5; h_1=71 (y_1=2.1); h_2=3 (y_2=1.0); *c*=5; *d*=16	*j*=1; *h*=60 (*y*=2.0); *c*=1; *b*=16; *d*=23
0.0	42.9	*j*=3; *h*=80 (*y*=2.1); *c*=16	*j*=8; *h*=75 (*y*=2.1); *c*=16	*j*=5; h_1=63 (y_1=2.1); h_2=4 (y_2=1.0); c=11; *d*=16	*h*=56 (*y*=2.0); *c*=13; *b*=11; *d*=20
0.0	53.9	*j*=3; *h*=74 (*y*=2.1); *c*=24	*j*=7; *h*=70 (*y*=2.1); *c*=23	*J*=4; *h*=62 (*y*=2.0); *c*=18; *d*=16	*h*=51 (*y*=2.0); *c*=19; *b*=10; *d*=20
0.0	66.7	*j*=3; *h*=67 (*y*=2.1); *c*=30	*j*=6; *h*=62; (*y*=2.1); *c*=32	*j*=4; *h*=47 (*y*=2.0); *c*=31; *d*=18	*h*=43 (*y*=2.0); *c*=29; *b*=10; *d*=18
0.0	81.8	*j*=2; *h*=60 (*y*=2.1); *c*=38	*j*=5; *h*=55 (*y*=2.1); *c*=40	*j*=3; *h*=49 (*y*=2.1); *c*=36; *d*=12	*h*=40 (*y*=2.0); *c*=35; *b*=8; *d*=16
0.0	100.0	*j*=2; *h*=55 (*y*=2.2); *c*=43	*j*=5; *h*=51 (*y*=2.2); *c*=44	*j*=3; *h*=44 (*y*=2.0); *c*=42; *d*=11	*h*=35 (*y*=2.0); *c*=42; *b*=8; *d*=15
12.5	12.5	*j*=7; *k*=26; *t*=12; *h*=49 (*y*=1.6); *c*=6	*j*=11; *h*=89 (*y*=1.5)	*j*=7; *h*=93 (*y*=1.4)	*p*=1; *j*=4; f=1; *x*=18; *h*=75 (*y*=1.3)
14.3	28.6	*j*=4; *k*=11; *t*=9; *h*=61 (*y*=1.6); *c*=14	*h*=88 (*y*=1.5); *c*=12	*j*=2; h_1=62 (y_1=1.4); h_2=31 (y_2=1.0); *c*=5	*p*=3; x=9; h_1=46 (y_1=1.2); h_2=33 (y_2=0.9); *c*=9
28.6	14.3	*t*=22; *x*=39; *h*=30 (*y*=1.4); *c*=10	*t*=10; *x*=38; *h*=48 (*y*=1.3); *c*=4	*x*=37; *h*=63 (*y*=1.0)	*x*=9; h_1=44 (y_1=1.2); h_2=35 (y_2=0.8); *c*=7; *b*=6
16.7	50.0	*j*=1; *t*=8; *h*=68 (*y*=1.5); *c*=23	*t*=6; *h*=67 (1.4); *c*=27	h_1=47 (y_1=1.5); h_2=35 (y_2=0.9); *c*=19	*x*=4; h_1=37 (y_1=1.1); h_2=36 (y_2=0.7); *c*=20; *b*=4
33.3	33.3	*t*=18; *x*=36;*h*=26 (*y*=1.4); *c*=20	*t*=7; *x*=40; *h*=34 (*y*=1.2); *c*=19	*x*=45; h_1=12 (y_1=1.1); h_2=21 (y_2=0.8); *c*=21	*x*=56; *h*=14 (*y*=0.8); *c*=30
50.0	16.7	*t*=19; *x*=64; *h*=5*; *c*=12	*x*=84; *c*=16	*x*=55; *v*=31; *c*=13	*x*=21; *v*=58; *h*=6 (*y*=1.8); *c*=14
20.0	80.0	*t*=9; *h*=54 (*y*=1.5); *c*=36	*t*=4; *x*=10; *h*=48 (*y*=1.3); *c*=38	*x*=3; h_1=35 (y_1=1.3); h_2=28 (y_2=0.9); *c*=33	*h*=65 (*y*=0.8); *c*=32; *b*=2
40.0	60.0	*t*=20; *x*=39; *h*=11*; *c*=31	*t*=8; *x*=55; *c*=38	*x*=51; *h*=13 (*y*=0.7); *c*=36	*x*=43; *v*=15; *c*=43
60.0	40.0	*t*=13; *x*=25; *g*=38; *c*=22	*x*=27; *g*=37; *v*=13; *c*=24	*x*=35; *v*=39; *c*=26	*x*=11; *v*=62; *c*=27
80.0	20.0	*g*=83; *q*=8; *c*=9	*g*=64; *v*=20; *q*=4; *c*=12	*x*=13; *v*=71; *q*=2; *c*=15	*x*=4; *v*=76; *q*=6; *c*=14

Codes for phases are given in Table 4. Where no *y* value is given for hydrogarnet (*) peak overlap prevented the estimation of *y* from *d*-spacing and a standard hydrogarnet structure was used to fit the hydrogarnet phase in order to estimate weight percent. Silica flour and coarse corundum are given in % by wt of cement (BWOC).

not necessarily reach phase equilibrium at the end of the 5 d curing period.

3. Analytical

A Bruker-AXS D8-series 2 X-ray powder diffractometer, running at 40 kV and 40 mA, was employed for mineralogical analysis. Incident Cu $K_{\alpha 1}$ radiation from a Ge monochromator was passed through a 2 mm monochromator exit slit and 0.2° divergence slit. A Braun position sensitive detector was used to collect data. Three types of scan were employed. Most diffraction patterns were collected over an angular range of 5 to 70° 2θ for approx 30 min total time using a step size of 0.014°2θ and a count time of 0.3 s per step. Where a more detailed scan was required, samples were run for 6 or 12 h over the same angular range using a smaller step size (0.007° 2θ) and longer count time (1.7 or 3.5 s per step, respectively). Finally, where large silica additions were made (>50% BWOC), samples were run at lower angles to confirm the presence or absence of gyrolite whose strongest peak lies at 4°2θ (2.2 nm).

Phases were identified using the powder diffraction database from the International Centre for Diffraction Data (ICDD) and the Bruker search-match software EVA. Once phases were identified they were quantified using Rietveld refinement methods using the Bruker fitting program TOPAS. Phase quantification using this method has been successful both on dry cement [19] and hydroceramics [12]. The method does however have its limitations. Every phase in the sample must be identified and the crystal structure for each phase must be known (Table 4). It is assumed the samples are wholly crystalline as no amorphous phases were detected either by spiking methods or le Bail silica curve fitting [20]. Where the crystal structure is not known (for example, for C_8S_5) the proportion of that phase must be estimated using spiking methods. Ten wt percent gypsum is added to our samples and the totals recalculated to estimate the final percentage of C_8S_5 and its co-existing phases. While a few percent error may normally be expected in association with any of the phases present in the hydroceramics, spiking methods obviously increase such errors and quantification by spiking methods should be treated with some caution.

With the presence of unknown errors associated with quantification by Rietveld refinement we might ask how we can even know whether the results are realistic. Mass balancing of simple phase assemblages by Meller et al. [12] suggests that the Rietveld refinement method yields accurate results. In addition we have compared the mole ratios C/(C+S) and C/(C+A) of the sample with the corresponding quantities from the Rietveld refinement (Fig. 2) and generally find good agreement. The C/(C+S) ratios are particularly close, differing by <10% for the most part. C/(C+A) ratios lie a little further from the 1:1 correlation line, particularly when higher proportions of corundum are added to the mix (>33% BWOC). Electron probe results (Table 5) show that the calcium/aluminum ratio of the hydrogarnet is not ideal (the C/(C+A) value is commonly ≥0.70). This has been taken into account in creating the plot but does not fully account for the shortfall

Table 3
Weight percent of phases present in each sample as estimated by Rietveld refinement

Initial composition % BWOC		Wt.% of phases in hydroceramics	
Silica flour	Fine corundum	200 °C	250 °C
0.0	11.1	–	p=5; j=11; h_1=57 (y_1=2); h_2=24 (y_2=2.4)
0.0	66.7	h=69 (y=2.1); c=31	–
12.5	12.5	–	j=9; h=90 (y=1.2)
14.3	28.6	–	t=9; h_1=28 (y_1=2.7); h_2=54 (y_2=1.3); c=9
28.6	14.3	t=46; h=54 (y=1.4); c=10	t=17; x=27; h=56*
16.7	50.0	t=18; h_1=29 (y=2.0); h_2=32 (y=1.4); c=21	t=9; h_1=36 (y_1=2.0); h_2=34 (y_2=1.4); c=21
33.3	33.3	t=49; q=3;h=36 (y=1.5); c=12	–
50.0	16.7	t=91; x=4; c=5	t=62; x=29; c=9
20.0	80.0	t=20; q=2; h=42 (y=1.9); c=36	t=12; h_1=41 (y_1=2.0); h_2=14 (y_2=1.9); c=33
40.0	60.0	t=42; q=5; h=26 (y=1.6); c=27	t=42; q=2; h=28 (y=1.4); c=28
60.0	40.0	t=58; q=9; h=17 (y=1.5); c=16	t=70; q=10; c=20
80.0	20.0	t=71; q=14; h=6*; c=9	t=68; q=20; c=10

Codes for phases are given in Table 4. Where no y value is given for hydrogarnet (*) peak overlap prevented the estimation of y from d-spacing and a standard hydrogarnet structure was used to fit the hydrogarnet in order to estimate weight percent. Silica flour and fine corundum are given in % by wt of cement (BWOC).

in alumina, suggesting that either corundum or hydrogarnet or both are being slightly overestimated by the Rietveld method.

4. The CASH hydroceramic system

4.1. High C/(C+S) hydrates: portlandite, jaffeite, reinhardbraunsite, hillebrandite and α-C_2SH

The high C/(C+S) (>0.5) hydrates occur with low silica and/or with low alumina additions (<25% BWOC). Jaffeite persists when more alumina is added but is generally present only in small amounts (typically a few percent). Of these hydrates, the formation of reinhardbraunsite (also known as calcio-chondrodite), hillebrandite and α-C_2SH are strongly temperature dependent, while portlandite and jaffeite are present over the complete temperature range (Figs. 3 and 4). Hillebrandite and α-C_2SH are found at 200 °C but not at higher temperatures. Taylor's diagram (Fig. 1) suggests that α-C_2SH is found only up to 150 °C, above which it is replaced by hillebrandite. Hillebrandite is observed as a minor phase in our system (<10%) whereas α-C_2SH is a major phase (60%), particularly at 5.3% BWOC silica addition (Table 2). Hillebrandite and α-C_2SH appear to be replaced by reinhardbraunsite above 200 °C.

4.2. C_8S_5

The CASH system at 200 °C has previously been fully described by Meller et al. [13,14]. The main difference to note here is that C_8S_5 was not previously identified in these samples and occurs when 11 to 33% of silica flour BWOC is added from 200 to 350 °C. C_8S_5 is poorly documented in the literature and no crystal structure refinement currently exists. A powder diffraction file does however exist in the JCPDS database (card no. 29-368) and its structure is believed to be related to kilchoanite and γ-C_2SH. Where it has been observed previously it is found coexisting with [21] or as a decomposition product of γ-C_2SH [22] and its XRD pattern typically shows it to be poorly crystalline compared to other calcium silicate (hydrate) products in hydroceramics (Fig. 5), thus accounting for its previous misidentification. While it is found only in samples with silica additions and not those with alumina additions it forms a significant proportion of the sample from 11 to 33% of silica flour BWOC from 200 to 350 °C (Table 2). We note that it is also absent from Taylor's diagram. It is possible that C_8S_5 is a metastable product in our system either because of the short curing period or because the impurities in the cement alter the phase boundaries of the pure system (compare Figs. 1 and 3).

4.3. 1.1 nm tobermorite

1.1 nm tobermorite coexists with C_8S_5 in the range of silica additions from 11 to 33% BWOC at 200 °C, and with xonotlite from 20 to 50% of silica additions BWOC. At 250 °C 1.1 nm tobermorite persists but only when 20 to 40% alumina BWOC is added (Fig. 6, Table 2). Taylor's diagram suggests that 1.1 nm tobermorite is found only to approx 150 °C but it is commonly reported in the literature that its temperature of stability can be raised by the addition of alumina [23–29]. The majority of samples were synthesised using a laboratory coarse alumina reagent; however in some cases the finer alumina was used (Table 3). The ternary contour plot in Fig. 6 shows the amount in weight percent of 1.1 nm tobermorite (calculated from Rietveld refinement) in samples made with coarse and fine alumina. The sample compositions (open circles) are expressed as molar proportions of the three major oxides present in the system CaO, SiO_2 and

Table 4
Phases identified in CASH hydroceramics synthesised at 200 to 350 °C, ICDD card numbers and structure references

Phase	Chemical formula	Cement notation	ICDD Card No	Crystal Structure Reference
Alpha dicalcium silicate hydrate; a	$Ca_2SiO_3(OH)_2$	α–C_2SH	29-373	Yano *et al.* [36]
Bicchulite; b	$Ca_8(Al_2SiO_6)_4(OH)_8$	$C_8A_4S_4H_4$	86-751	Dann *et al.* [37]
Calcium alumina hydrate; d	$Ca_4Al_6O_{13}{\cdot}3H_2O$	$C_4A_3H_3$	14-464	Ponomarev *et al.* [38]
Calcium silicate; m	$Ca_8Si_5O_{18}$	C_8S_5	29-368	None exists
Corundum; c	Al_2O_3	A	42-1468	Not referenced
Foshagite; f	$Ca_4(Si_3O_9)(OH)_2$	C_4S_3H	74-360	Gard and Taylor [39]
Gyrolite; g	$Ca_{16}Si_{24}O_{60}(OH)_8{\cdot}(14+n)H_2O$ $0\le n\le 3$	$C_{16}S_{24}H_{18+n}$ $0\le n\le 3$	42-1452	Merlino [40]
Hillebrandite; l	$Ca_2(SiO_3)(OH)_2$	C_2SH	42-538	Dai and Post [41]
Hydrogarnet; h	$Ca_3Al_2(SiO_4)_{3-y}(OH)_{4y}$ $0\le y\le 3$	$C_3AS_{3-y}H_{2y}$ $0\le y\le 3$	Hibschite 45-1447 Katoite 38-368	Cohen-Addad *et al.* [34] Sacerdoti and Passaglia [33]
Jaffeite; j	$Ca_6(Si_2O_7)(OH)_6$	$C_6S_2H_3$	29-375	Yamnova *et al.* [42]
Kilchoanite; k	$Ca_6(SiO_4)(Si_3O_{10})$	C_6S_4	11-316	Taylor [43]
Portlandite; p	$Ca(OH)_2$	CH	4-733	Petch [44]
Quartz; q	SiO_2	S	33-1161	Not referenced
Reinhardbraunsite; r	$Ca_5(SiO_4)_2(OH)_2$	C_5S_2H	29-380	Kuznetsova *et al.* [45]
1.1 nm Tobermorite; t	$Ca_5Si_6O_{17}{\cdot}5(H_2O)$	$C_5S_6H_5$	19-1364	Merlino *et al.* [46]
Truscottite; v	$Ca_{14}Si_{24}O_{62}{\cdot}(4+z)H_2O$ $0<z<6$	$C_{14}S_{24}H_{4+z}$ $0<z<6$	29-382	Merlino [47] (truscottite structure based on modified reyerite structure)
Xonotlite; x	$Ca_6Si_6O_{17}(OH)_2$	C_6S_6H	29-379	Mamedov and Belov [48]

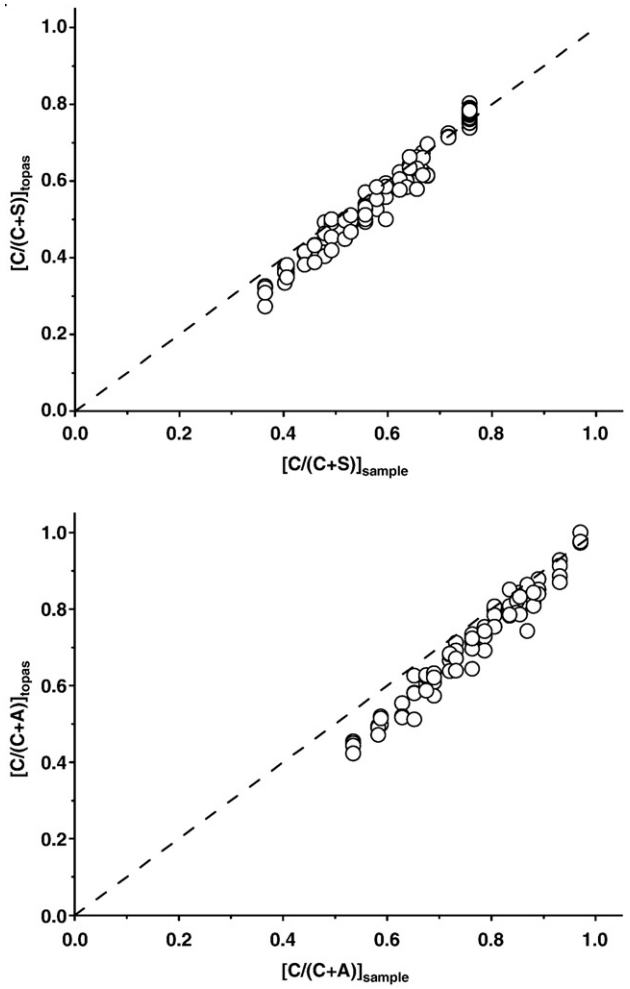

Fig. 2. Comparisons of mol ratios C/(C+S) and C/(C+A) of the bulk sample and the phase assemblages quantified by Rietveld refinement (Table 2).

Al_2O_3. The calculated molar proportions of SiO_2 and Al_2O_3 include the amount of these oxides from the cement, and the amount added to each sample. It is clear that finer alumina promotes the formation of 1.1 nm tobermorite.

Table 5
Electron microprobe analyses of selected hydrogarnets showing that C/(C+A) is in range 0.65–0.67

	200 °C		300 °C	
Wt per cent of oxides				
CaO	44.49	44.13	40.68	41.80
SiO_2	17.52	16.79	15.44	15.51
Al_2O_3	20.45	21.62	19.68	18.17
MgO	0.44	0.28	0.70	0.61
Fe_2O_3	1.16	0.65	3.30	3.45
SO_3	2.11	0.73	1.22	1.78
H_2O	13.16	15.80	18.88	18.41
Formula based on 12 oxygens				
Ca	3.300	3.276	2.910	3.015
Si	1.230	1.163	1.030	1.044
Al	1.693	1.766	1.548	1.441
Mg	0.046	0.030	0.069	0.061
Fe^{3+}	0.061	0.034	0.165	0.174
S	0.111	0.060	0.060	0.090
H	6.181	6.846	8.378	8.222
y	1.77	1.83	1.97	1.94
C/(C+A)	0.66	0.65	0.65	0.67

Samples contain 25% corundum BWOC.

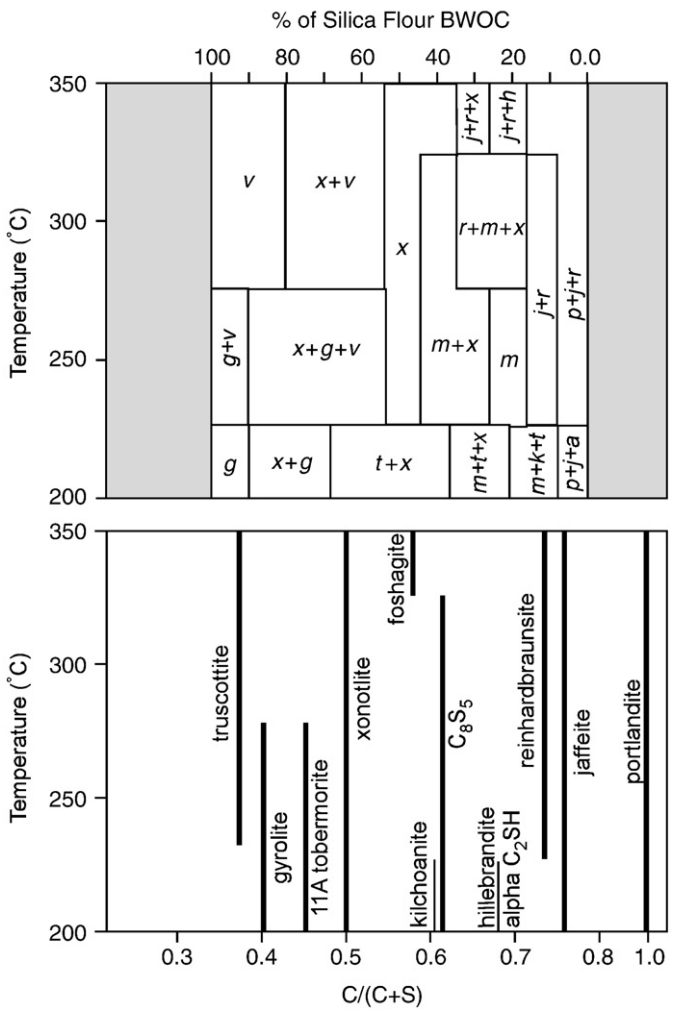

Fig. 3. Phase diagram (lower figure) and phase map (upper figure) for the cement and silica flour system from 200 to 350 °C. The phase diagram shows the temperatures over which phases > 10 wt.% are present. The phase map illustrates which major phases form for different proportions of silica flour in % BWOC. Abbreviations for phases are given in Table 4. Shaded area represents compositions not investigated here.

Tobermorite is commonly reported as having a higher compressive strength and lower permeability than xonotlite [6,29,30] and so the prevalence of tobermorite in our hydroceramics suggests that the addition of alumina improves the engineering properties of the sealant, although further testing is required. We have not been able to establish which form of 1.1 nm tobermorite is present. It has long been known that two forms of 1.1 nm tobermorite exist: normal and anomalous [9,31]. Normal 1.1 nm tobermorite collapses on heating to 0.9 nm tobermorite whereas anomalous 1.1 nm tobermorite persists to higher temperatures, its structure being supported by ions, e.g. Al^{3+}, which are not present in the normal structure. While it has not been possible to establish conclusively which form is present from the XRD patterns it is more than likely that the anomalous form is present as the presence of small amounts of additional alumina appear to encourage its formation.

4.4. Xonotlite

Xonotlite is present over the entire range of temperatures examined when silica flour additions exceed 11% BWOC and our results are in accordance with those of Roy et al.[17] who studied similar systems. The presence of alumina does not appear to increase the proportion of xonotlite formed, in contrast to the case of tobermorite. This is consistent with earlier observations [32]. However the field of stability does appear

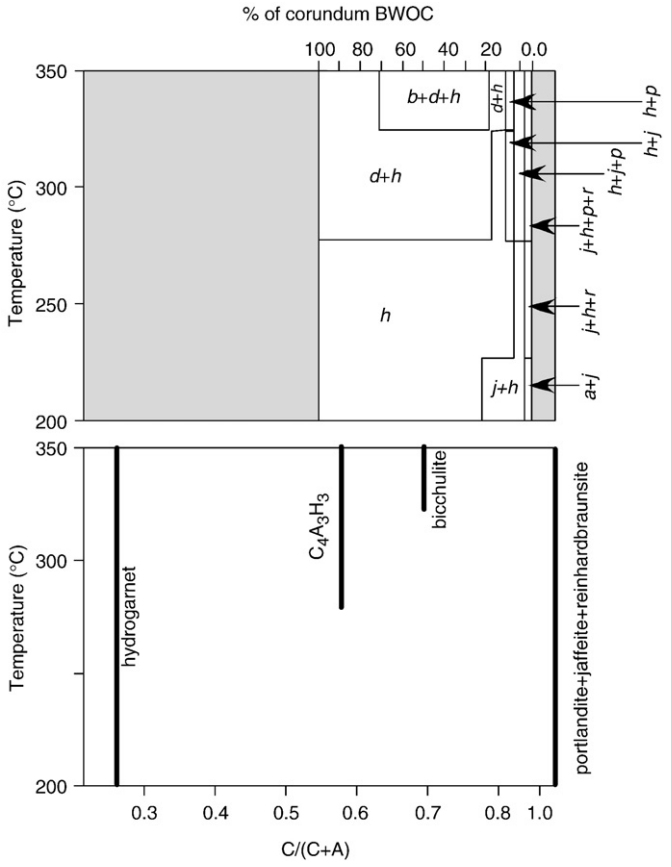

Fig. 4. Phase diagram (lower figure) and phase map (upper figure) for the cement and corundum system from 200 to 350 °C. The phase diagram illustrates the temperatures over which phases >10 wt.% are present. The phase map shows which major phases form for different proportions of corundum in % BWOC. Abbreviations for phases are given in Table 4. Shaded area represents compositions not investigated here.

to shift to higher C/(C+S) at 350 °C, perhaps as a result of a lack of C_8S_5 at this temperature (Table 2).

4.5. Low C/(C+S) hydrates: gyrolite and truscottite

The low C/(C+S) phases form when silica additions exceed 40% BWOC. We find that gyrolite and truscottite coexist at 250 °C, below

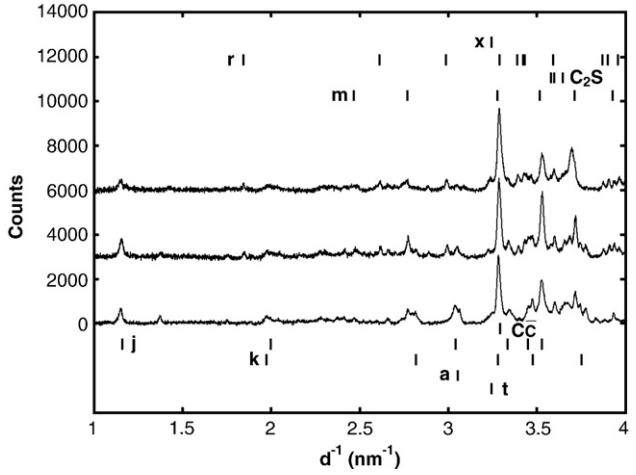

Fig. 5. XRD pattern of cement with 11% of silica flour BWOC at 200 (lower), 250 (middle) and 300 (upper) °C illustrating presence of C_8S_5 (m), kilchoanite (k), jaffeite (j), α-C_2SH (*a*), 1.1 nm tobermorite (t), reinhardbraunsite (r), xonotlite (x), calcite ($C\bar{C}$) and relict belite (β-C_2S) and the poorly crystalline nature of the product phases.

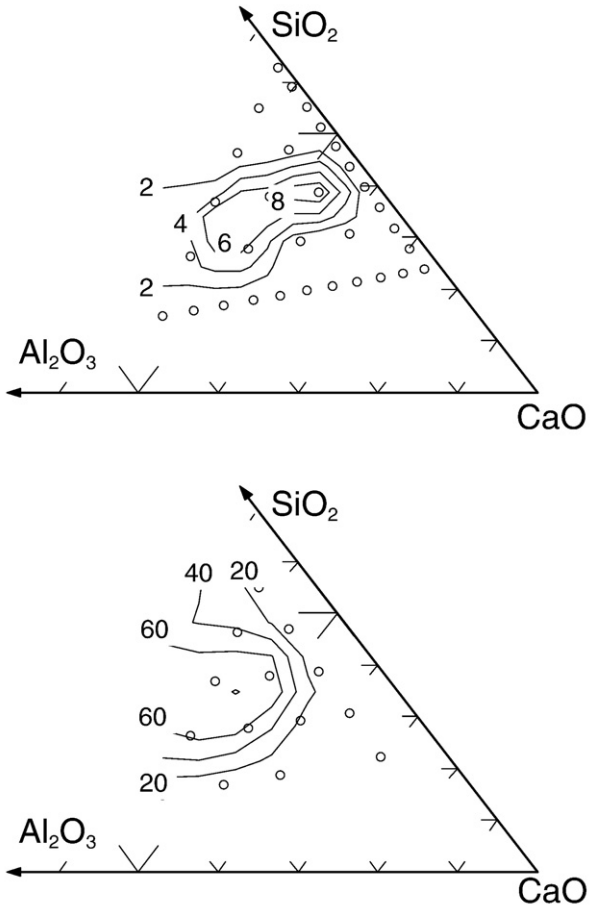

Fig. 6. Ternary plots of wt.% 1.1 nm tobermorite with coarse (upper figure) and fine (lower figure) corundum. Sample points (open circles) are plotted as molar proportions of CaO, SiO_2 and Al_2O_3. Tick marks are at intervals of 0.1.

which only gyrolite is present and above which only truscottite is found (Fig. 3). Taylor's diagram (Fig. 1) on the other hand indicates that gyrolite is replaced by truscottite at about 200 °C. It is possible that our system has not reached phase equilibrium. We also note that the proportion of gyrolite in samples cured at 250 °C is increased by the addition of alumina at lower silica contents, probably by the incorporation of alumina in the structure (K. Kyritsis unpublished data). This effect is also observed for truscottite but not to such a great extent.

4.6. Hydrogarnet

Hydrogarnet is the most common aluminum-bearing secondary phase produced in the system we have studied. It is most abundant when corundum is added but is present in all samples except those with silica only additions exceeding 11% BWOC. To quantify hydrogarnet two patterns were used as this mineral displays solid solution from grossular ($y=0$) to katoite ($y=3$), the general formula being $C_3AS_{3-y}H_{2y}$. The y value is determined by measuring the *d*-spacing of the hydrogarnet peaks [12] and from this occupancy factors are determined for Si and H which are fed into the refinement process. Two structures are used: the Sacerdoti [33] katoite structure as default but where the y value is significantly low (<0.8) the Cohen-Addad [34] hibschite structure is used. In some samples above 250 °C more than one hydrogarnet is present (Fig. 7) and both structures can be fitted. The lower pattern in Fig. 7 corresponds to a sample made using coarse alumina, cured at 350 °C, with the y values of the two different hydrogarnets being 1.2 (Sacerdoti structure used) and 0.8 (Cohen-

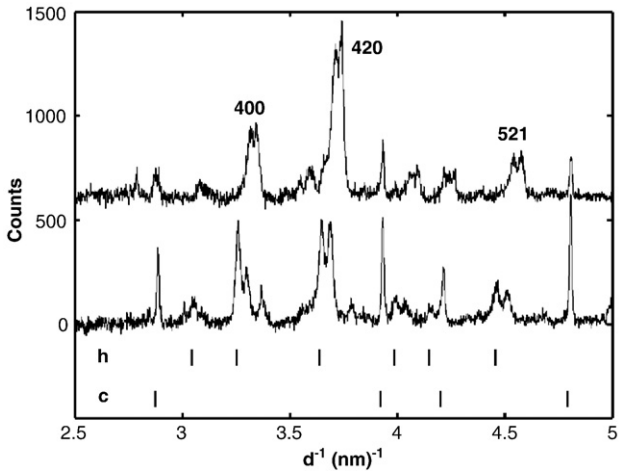

Fig. 7. Samples illustrating presence of two distinct hydrogarnets (*h*) with split 400, 420 and 521 peaks. Some relict corundum is present (*c*). The lower sample was synthesised at 200 °C and contains 16.7% of silica flour and 50% of fine corundum BWOC. The upper sample was synthesised at 350 °C and contains 28.6% of silica flour and 14.3% of corundum BWOC.

Addad structure used) respectively (Table 2). The addition of fine alumina appears to promote the formation of two distinct hydrogarnets at lower temperatures. The upper pattern in Fig. 7 illustrates a sample made using fine alumina, cured at 200 °C, with the *y* values being 2 and 1.4 respectively (Table 3). It may well be possible that the broad peaks observed for hydrogarnets, where only one composition is observed, may indeed represent a range of compositions and our estimate of *y* represents an average composition for the sample [35].

The *y* value of hydrogarnet is perhaps more strongly influenced by the system composition, *y* decreasing as silica is added (Fig. 8). This suggests that given sufficient alumina to nucleate and grow the hydrogarnet, the overall composition depends on the amount of silica in the system. In addition to this the temperature also appears to influence *y*, a tendency to move towards lower *y* at higher temperatures being observed. Whether this is because the upper temperature limit of katoitic hydrogarnet is being approached or the calcium, aluminum and water are entering a new phase ($C_4A_3H_4$ or bicchulite) above 250 °C (Fig. 4) is unclear.

However the presence of hydrogarnets in minor or trace amounts in samples with silica-only additions less than 11% BWOC is problematic as the peaks overlap with relict C_2S. This makes Rietveld refinement impossible, especially at temperatures <300 °C. Hence although we can see small identifiable hydrogarnet peaks in these samples we cannot fit them at present and must treat hydrogarnet as zero in the quantified sample (Table 2).

4.7. Other phases

Not all the phases present have been described above. Relict corundum and silica are observed in some samples, particularly where additions are high (Table 2). Higher temperature does not appear to increase corundum consumption but silica consumption does increase with increasing temperature. However it also appears that further additions of either silica or corundum add little value to the product as relict corundum or quartz are observed in the diffraction pattern. Indeed it seems that additions of >50% of corundum BWOC add little value in terms of product phases.

Other phases present either in small quantities or in a few samples include kilchoanite and foshagite. Kilchoanite is observed in four samples (Fig. 5, Table 2) at 200 °C. This is at odds with Taylor's diagram (Fig. 1) where it is observed in the pure system at temperatures only in excess of 500 °C. However Taylor [9] stated that kilchoanite has been noted with other products formed by hydrothermal treatment of afwillite at temperatures little above 200 °C. Therefore the presence of this anhydrous mineral in hydroceramics should be expected. It is probably a metastable phase in our system because of the short curing period.

Foshagite is observed in two samples at 350 °C (Table 2). According to Taylor's diagram it would be expected at lower temperatures than this but its formation is probably being prevented by the presence of C_8S_5 whose C/S ratio is not dissimilar (0.57 vs. 0.62).

Finally there was no evidence from the X-ray diffraction patterns of the existence of sulphate phases. Electron microprobe results (K. Kyritsis, unpublished data) show that the sulphate originally present in the cement is incorporated in product phases such as jaffeite, reinhardbraunsite, xonotlite, gyrolite and hydrogarnets [35].

4.8. Cautionary notes

Small amounts of carbonate (calcite $C\bar{C}$) are observed in most samples (Fig. 5). The carbon dioxide from the air in the autoclave is not sufficient to form the amounts observed (typically <10%). Therefore the carbonate must result either from the water used (which was not deaerated) or from exposure to the atmosphere during cooling and dehydration. Although samples were dried under vacuum we were unable to completely prevent the formation of carbonate. The carbonate is not quantified for simplicity, hence small mismatches in C/(C+S) or C/(C+A) may also be explained by the presence of minor or trace amounts of carbonate in the system.

Unreacted belite β-C_2S is also present in some samples (Fig. 5). Quantification of this phase in the hydrated samples is difficult as

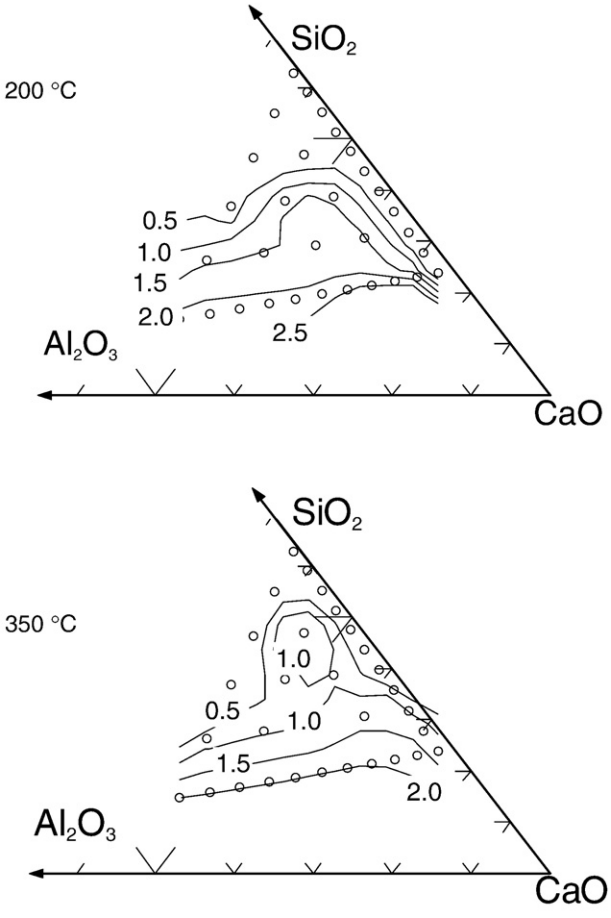

Fig. 8. Ternary contour plots of the hydrogarnet *y* parameter illustrating a shift towards more grossular-rich hydrogarnets as temperature is increased. Sample points (open circles) are plotted as molar proportions of CaO, SiO_2 and Al_2O_3. Tick marks are at intervals of 0.1.

peaks are broad, and frequently overlap peaks from other phases, notably those of hydrogarnet. Partial C_2S hydrates have been observed using the electron microprobe (e.g. C_4S_2H) but no satisfactory ICDD patterns or crystal structures exist for these phases. Once again for simplicity and because of fitting difficulties the relict C_2S phase has not been quantified.

With regards to phase identification, not all peaks can satisfactorily be identified. The system is extremely complex, sometimes containing five or more product phases (Fig. 5, Table 2). We have already noted many differences between the stability fields of the pure system (Fig. 1) and the samples synthesised with real cement. It is unlikely that we have always succeeded in identifying every phase which can form under hydrothermal conditions in the CASH system. Lastly it should be noted that the samples used in this study were only hydrated for 5 d. Samples synthesised over shorter periods of time [12] do display intermediate products and it is uncertain at present whether all the phases found in these samples are the final product phases or are intermediate phases of a much longer hydration process.

5. Conclusions

We have compared the pure C–S system of Taylor (Fig. 1) with that produced from a system consisting of cement and silica (Fig. 3) more representative of practical formulations over the temperature range 200 to 350 °C. While many phases appear to be stable at similar temperatures (portlandite, jaffeite, hillebrandite, reinhardbraunsite and xonotlite) there are numerous deviations from the pure system when using real cements:

The stability of α-C_2SH is extended to at least 200 °C.

C_8S_5, not observed by Taylor, forms a large proportion of the sample from 11 to 33% of silica flour BWOC.

The stability of 1.1 nm tobermorite is greatly extended from 170 °C towards 300 °C.

When alumina is added to the system, not only are aluminum bearing phases dominant (Fig. 4), but the stability fields of nominally Al-free phases are extended, both in terms of composition and temperature range. Thus:

Hydrogarnet is the dominant Al-bearing product phase in the system. The broad peaks suggest that a range of compositions is present within any one sample and some samples display more than one distinct composition.

The composition of hydrogarnet appears to depend on the C/S ratio of the sample and temperature, *y* decreasing with decreasing C/S and increasing temperature.

At >250 °C hydrogarnet is replaced by $C_4A_3H_3$.

At >300 °C hydrogarnet is replaced by both $C_4A_3H_3$ and bicchulite.

The presence of alumina, particularly fine grained alumina, pushes the stability fields of 1.1 nm tobermorite and gyrolite to higher temperatures.

Acknowledgements

We thank the UK EPSRC for financial support and for the use of the Chemical Database Service at Daresbury. We also thank Dyckerhoff and Sibelco for donating materials.

References

[1] D.A.C. Manning, P.L. Younger, F.W. Smith, F.W. Jones, J.M. Jones, D.J. Dufton, S. Diskin, A deep geothermal exploration well at Eastgate, Weardale, UK: a novel exploration concept for low-enthalpy resources, Journal of the Geological Society, London 164 (2) (2007) 371–382.
[2] K.E. Rollin, A simple heat-flow quality function and appraisal of heat-flow measurements and heat-flow estimates from the UK Geothermal Catalogue, Tectonophysics 244 (1995) 185–196.
[3] P. MacDonald, A. Stedman, G. Symons, The UK geothermal hot dry rock R&D programme, in: H.J. Ramey, R.N. Horne, W.E. Brigham, J.W. Cook (Eds.), Proceedings of the 17th Workshop on Geothermal Reservoir Engineering, Stanford University, Stanford, CA, 1992, pp. 5–11.
[4] G.C. Brown, J. Plant, M.K. Lee, Geochemical and geophysical evidence on the geothermal potential of Caledonian Granites in the UK, Nature 280 (1979) 129–131.
[5] J.D. Garnish, Geothermal energy and the UK, Physics Education 13 (1978) 372–379.
[6] E. Nelson, Well Cementing, Schlumberger Educational Services, Sugar Land, Texas, 1990.
[7] K. Kyritsis, C. Hall, D. P. Bentz, N. Meller, M. A. Wilson, Relationship between engineering properties, mineralogy and microstructure in cement based hydroceramic materials cured at 200 °C to 350 °C (submitted to Journal of the American Ceramic Society).
[8] G. Carter, D.K. Smith, Properties of cementing compositions at elevated temperatures and pressure, Transactions of the Metallurgical Society of the American Institute of Metallurgical Engineers 213 (2) (1958) 20–26.
[9] H.F.W. Taylor, The calcium silicate hydrates, in: H.F.W. Taylor (Ed.), The Chemistry of Cements, vol. 1, Academic Press, London, 1964, pp. 168–232.
[10] V. Barlet-Gouédard, S. Danican, E. Nelson, C. Cambus, Cement Compositions for High Temperature Applications, PCT Patent Application WO 03/068708, 21 August 2003.
[11] V. Barlet-Gouédard, B. Vidick, A non-conventional way of developing cement slurry for geothermal wells, Geothermal Resources Council Transactions 25 (2001) 85–91.
[12] N. Meller, C. Hall, K. Kyritsis, G. Giriat, Synthesis of cement based $CaO–Al_2O_3–SiO_2–H_2O$ (CASH) hydroceramics at 200 and 250 °C: Ex-situ and in-situ diffraction, Cement and Concrete Research 37 (6) (2007) 823–833.
[13] N. Meller, C. Hall, J. Phipps, A new phase diagram for the $CaO–Al_2O_3–SiO_2–H_2O$ hydroceramic system at 200 °C, Materials Research Bulletin 40 (5) (2005) 715–723.
[14] N. Meller, C. Hall, Hydroceramic sealants for geothermal wells, in: M. Pecchio, F.R.D. Andrade, L.Z.D. D'Agostino, H. Kahn, L.M. Sant'Agostigno, M.M.M.L. Tassinari (Eds.), Proceedings of the International Congress on Applied Mineralogy, Sao Paolo, Brazil, 2004, pp. 281–284.
[15] E.L. White, C.A. Langton, M.W. Grutzeck, D.M. Roy, High temperature cements for geothermal applications, American Ceramic Society Bulletin 58 (3) (1979) 334.
[16] D.M. Roy, C.A. Langton, M.W. Grutzeck, E.L. White, Hydrothermal high temperature cements for potential geothermal applications, Proceedings of the 5th International Symposium on Oilfield and Geothermal Chemistry, Stanford, California, 1980, SPE 8994.
[17] D.M. Roy, E.L. White, C.A. Langton, M.W. Grutzeck, Potential new high temperature cements for geothermal wells, Proceedings of the International Symposium on Oilfield and Geothermal Chemistry, Houston, Texas, 1979, SPE 7877.
[18] C. Hall, K.L. Scrivener, Oilwell cement clinkers – X-ray microanalysis and phase composition, Advanced Cement Based Materials 7 (1) (1998) 28–38.
[19] K.L. Scrivener, T. Fullmann, E. Gallucci, G. Walenta, E. Bermejo, Quantitative study of Portland cement hydration by X-ray diffraction/Rietveld analysis and independent methods, Cement and Concrete Research 34 (9) (2004) 1541–1547.
[20] A. Le Bail, Modelling the silica glass structure by the Rietveld method, Journal of Non-Crystalline Solids 183 (1-2) (1995) 39–42.
[21] J.M. Bennet, J.A. Gard, K. Speakman, H.F.W. Taylor, $Ca_8Si_5O_{18}$ and the nature of γ-dicalcium silicate hydrate, Nature 209 (1966) 1127.
[22] X. Hu, K. Yanagisawa, A. Onda, K. Kajiyoshi, Effects of hydrothermal process on formation of calcium silicate hydrates at 250 °C, Journal of the Society of Inorganic Materials, Japan 13 (320) (2006) 32–39.
[23] N. Meller, C. Hall, K. Kyritsis, G. Giriat, H.J. Jakobsen, J. Skibsted, Incorporation of aluminium guest ions in nominally alumina-free calcium silicate hydrates: effects on crystal structure and thermal stability, in: J.J. Beaudoin, J.M. Makar, L. Raki (Eds.), Proceedings of the 12th International Congress on the Chemistry of Cement, Montreal Canada, 2007.
[24] F. Liu, D. Chen, W. Ni, Z. Cao, Effect of Al^{3+} on tobermorite crystallinity, Journal of University of Science and Technology Beijing 7 (2) (2000) 79–81.
[25] D.S. Klimesch, A.S. Ray, DTA-TGA evaluations of the $CaO–Al_2O_3–SiO_2–H_2O$ system treated hydrothermally, Thermochimica Acta 334 (1-2) (1999) 115–122.
[26] D.S. Klimesch, A.S. Ray, Effects of quartz particle size on hydrogarnet formation during autoclaving at 180 °C in the $CaO–Al_2O_3–SiO_2–H_2O$ system, Cement and Concrete Research 28 (9) (1998) 1309–1316.
[27] N. Isu, H. Ishida, T. Mitsuda, Influence of quartz particle size on the chemical and mechanical properties of autoclaved aerated concrete. 1. Tobermorite formation, Cement and Concrete Research 25 (2) (1995) 243–248.
[28] T. Sugama, L.E. Kukacka, W. Horn, Effects of tobermorite and calcium silicate hydrate (I) crystals formed within polymer concretes, Journal of Materials Science 16 (1981) 345–354.
[29] G.L. Kalousek, S.L. Chow, Research on cements for geothermal and deep oil wells, Society of Petroleum Engineers of AIME SPE 5940 (1976).
[30] L.D. Sanders, W.J. Smothers, Effect of tobermorite on the mechanical strength of autoclaved Portland cement-silica mixtures, Journal of the American Concrete Institute 28 (1957) 127–134.
[31] S. Merlino, E. Bonaccorsi, T. Armbruster, The real structure of tobermorite 11Å: normal and anomalous forms, OD character and polytypic modifications, European Journal of Mineralogy 13 (3) (2001) 577–590.
[32] K. Luke, H.F.W. Taylor, G.L. Kalousek, Some factors affecting formation of truscottite and xonotlite at 300–350 °C, Cement and Concrete Research 11 (2) (1981) 197–203.

[33] M. Sacerdoti, E. Passaglia, The crystal-structure of katoite and implications within the hydrogrossular group of minerals, Bulletin de Mineralogie 108 (1985) 1–8.
[34] C. Cohen-Addad, P. Ducros, E.F. Bertaut, Etude de la substitution du groupement SiO_4 par $(OH)_4$ dans les composés $Al_2Ca_3(OH)_{12}$ et $Al_2Ca_3(SiO_4)_{2.16}(OH)_{3.36}$ de type grenat, Acta Crystallographica 23 (1967) 220–230.
[35] K. Kyritsis, N. Meller, C. Hall, Chemistry and morphology of hydrogarnets formed in cement pastes cured at 200 °C to 350 °C, (Journal of the American Ceramic Society, in press).
[36] T. Yano, K. Urabe, H. Ikawa, T. Teraushi, N. Ishizawa, S. Udagawa, Structure of alpha dicalcium silicate hydrate, Acta Crystallographica C49 (1993) 1555–1559.
[37] S.E. Dann, P.J. Mead, M.T. Weller, Loewenstein's rule extended to an aluminium rich framework. The structure of bicchulite, $Ca_8(Al_2SiO_6)_4(OH)_8$, by MAS NMR and neutron diffraction, Inorganic Chemistry 35 (6) (1996) 1427–1428.
[38] V.I. Ponomarev, D.M. Kheiker, N.V. Belov, Crystal structure of tetracalcium trihydrotrialuminate $C_4A_3H_3$, Doklady Akademii Nauk SSSR 194 (1970) 1072–1075.
[39] J.A. Gard, H.F.W. Taylor, The crystal structure of foshagite, Acta Crystallographica 13 (1960) 785–793.
[40] S. Merlino, Gyrolite: its crystal structure and crystal chemistry, Mineralogical Magazine 52 (366) (1988) 377–387.
[41] Y. Dai, J.E. Post, Crystal-structure of hillebrandite: a natural analogue of calcium silicate hydrate (CSH) phases in Portland cement, American Mineralogist 80 (7-8) (1995) 841–844.
[42] N.A. Yamnova, K.H. Sarp, Y.K. Egorov-Tismenko, Y.D. Pushcharovski, G. Dasgupta, Crystal structure of jaffeite, Crystallography Reports 38 (4) (1993) 464–467.
[43] H.F.W. Taylor, The crystal structure of kilchoanite, $Ca_6(SiO_4)(Si_3O_{10})$, with some comments on related phases, Mineralogical Magazine 38 (293) (1971) 26–31.
[44] H.E. Petch, The hydrogen positions in portlandite, $Ca(OH)_2$, as indicated by the electron distribution, Acta Crystallographica 14 (9) (1961) 950–957.
[45] T.P. Kuznetsova, N.N. Nevskii, V.V. Ilyukin, N.V. Belov, Refinement of the crystal-structure of calcium chondrodite $Ca_5[SiO_4]_2(OH)_2$=$Ca(OH)_2 \cdot 2CaSiO_4$, Kristallografiya 25 (1) (1980) 159–160.
[46] S. Merlino, E. Bonaccorsi, T. Armbruster, Tobermorites: Their real structure and order-disorder (OD) character, American Mineralogist 84 (10) (1999) 1613–1621.
[47] S. Merlino, The structure of reyerite, $(Na, K)_2Ca_{14}Si_{22}Al_2O_{58}(OH)_8(H_2O)_2$, Mineralogical Magazine 52 (365) (1988) 247–256.
[48] K.S. Mamedov, N.V. Belov, The crystal structure of the minerals of the wollastonite group. 1. Structure of xonotlite, Zapiski Vsesoyuznogo Mineralogicheskogo Obshchestva 85 (1956) 13–38.